THE JOURNAL OF PHYSICAL CHEMISTRY C
A JOURNAL OF THE AMERICAN CHEMICAL SOCIETY

pubs.acs.org/JPCC

Article

Probing Activities of Individual Catalytic Nanoflakes by Tunneling Mode of Scanning Electrochemical Microscopy

Tianyu Bo, Xiang Wang, Rui Jia, Lili Han, Huolin L. Xin, Hanyu Zhang, Elisa M. Miller, and Michael V. Mirkin*

Cite This: https://doi.org/10.1021/acs.jpcc.1c07309

Read Online

ACCESS | Metrics & More | Article Recommendations

ABSTRACT: The tunneling mode of scanning electrochemical microscopy (SECM) was developed recently and applied to studies of charge-transfer reactions at single metal nanoparticles (NPs). When an scanning electrochemical microscope tip is brought within the tunneling distance from a conductive NP, the particle begins to act as a part of the nanoelectrode. Herein, we demonstrate the possibility of using carbon nanoelectrodes with a very thin insulating sheath for electrochemical tunneling experiments at flat samples. In this way, electrocatalytic activity, conductivity, and charging properties of and faradaic processes in layered nanomaterials can be characterized by single-nanoflake voltammetry without making direct ohmic contact with them. A broad applicability of tunneling SECM experiments is demonstrated by probing nanomaterials with different size, geometry, and electrocatalytic properties, including metallic/pseudo-metallic (1T/1T′) and semiconducting (2H) MoS_2 nanoflakes, N-doped porous carbon catalyst, and MXene nanosheets. The Tafel plots for the hydrogen evolution reaction (HER) and oxygen evolution reaction (OER) at individual nanoflakes are compared to analogous measurements for an ensemble of flakes attached to the surface of a macroscopic electrode. Moreover, we observed variations in catalytic activities of individual MXene flakes toward HER and OER caused by non-uniform doping.

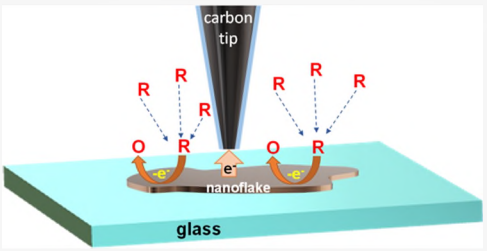

INTRODUCTION

Scanning electrochemical microscopy (SECM) is a powerful tool for studying heterogeneous charge-transfer processes and mapping surface reactivity at the nanoscale.[1−3] Two widely used classical modes of the SECM operation—feedback mode and generation/collection mode—are based on diffusion of redox species between the tip and sample surface.[4] These modes of SECM are applicable when reactants, products, and/or intermediates of an investigated process are electroactive and can be oxidized or reduced at the tip nanoelectrode. Many electrocatalytic reactions do not belong to this category and cannot be studied by either feedback or generation/collection mode of SECM. For example, electrochemical mapping of catalytic reduction of CO_2 could only be performed by scanning electrochemical cell microscopy (SECCM[5]) that employs a nanopipette to read the local substrate current.[6] However, SECCM may not be suitable for probing some of the samples discussed in the present article (see below).

In addition to the abovementioned limitation, the diffusion of electroactive species in the tip/substrate gap limits the attainable lateral resolution of SECM imaging to the value comparable to the tip radius (for discussion, see ref 7). A much higher resolution can be obtained by eliminating diffusion in the tip/substrate gap. We have recently introduced the tunneling mode of SECM and showed that it can be used for probing heterogeneous reactions at single nanoparticles[8,9] and electrochemical imaging with extremely high lateral resolution (*ca.* 1 nm[10]). In these experiments, an SECM tip is brought within a ≤2−3 nm distance from the surface of a conductive nanoscale sample (*e.g.*, a metal NP, Scheme 1A) attached to a macroscopic insulating support, and the source of the tip current (i_T) is electron tunneling between the tip and the nano-sample rather than the diffusion of redox species in the gap between them. Unlike conventional tunneling experiments (*e.g.*, STM junctions[11] and electrochemical STM[12−14]), in the tunneling mode of SECM, no voltage is applied between the tip and the substrate, and the tip current at short separation distances is due to the electrochemical reaction occurring at the nano-sample surface (Scheme 1A). As an SECM tip approaches a conductive particle attached to an insulating support, the tunneling resistance decreases exponentially with decreasing separation distance (d), and the tip potential begins to drive the charge-transfer process at the NP/solution interface.[8,9] The particle potential changes over ~2 nm tip displacement from the open circuit value to the tip

Received: August 18, 2021
Revised: October 27, 2021

Scheme 1. Schematic Representation of the Tunneling Mode SECM Experiment with a Polished Metal Tip at a Single NP (A) and an Attempt to do a Similar Experiment at a Flat Sample (B). The figure is not drawn to scale

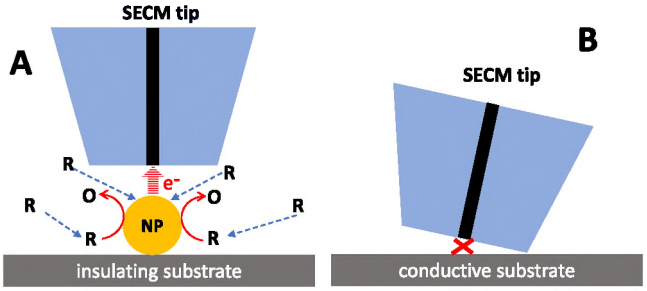

potential (E_T) value, and the metal NP begins to act as a part of the nanoelectrode. In tunneling regime, the tip current is due to the electrochemical reaction at the NP surface (*e.g.*, oxidation of the reduced species, *R*, present in solution; Scheme 1A), and its magnitude is determined by the diffusion flux of *R* molecules to the nano-specimen. In this way, voltammograms at a single NP can be recorded without attaching it to the electrode surface.

In previous tunneling SECM experiments, a glass-sealed disk-type tip was brought within the tunneling distance from a spherical[8,9] or cubic[10] NP whose top was a few nm above the underlying flat surface (Scheme 1A). By contrast, electrochemical tunneling experiments at a flat sample (or a nanorod) are challenging because any deviation from the perfect tip/substrate alignment results in the relatively thick glass insulator touching the sample surface before the conductive disk comes sufficiently close to it (Scheme 1B). Here, we show that carbon nanoelectrode (CNE) tips, having a thin glass insulator,[15] can be employed for electrochemical tunneling experiments at flat samples. In this way, the tunneling mode of SECM can be used to investigate a wide range of layered nanomaterials and 2D electrocatalysts.

■ METHODS

Chemicals and Materials. Ferrocyanide (99%), KCl (99%), $HClO_4$ (70%), and $NaClO_4$ (99%) were purchased from Sigma-Aldrich. Ferrocenemethanol (Fc; 99%, Sigma-Aldrich) was sublimed before use. All aqueous solutions were prepared using deionized water from the Milli-Q Advantage A10 system (Millipore Corp.) equipped with Q-Gard T2 Pak, a Quantum TEX cartridge, and a VOC Pak with total organic carbon ≤ 1 ppb. A 3 mm glassy carbon disk electrode was purchased from Bioanalytical Systems.

Fabrication of Carbon Nanotips. CNEs were prepared by chemical vapor deposition of carbon inside pre-pulled quartz nanopipettes, as described previously.[16,17] Briefly, nanopipettes were prepared by pulling quartz capillaries (1.0 mm o.d., 0.5 mm i.d.; Sutter Instrument Company) with a laser pipette puller (P-2000, Sutter Instruments). The following pulling parameters have been used:

	heat	filament	velocity	delay	pull
step 1	720	3	22	135	90
step 2	705	2	47	128	110

Carbon was deposited onto the inner pipette wall by chemical vapor deposition (CVD) at 950 °C, using methane as a carbon source and argon as a protector (argon/methane: 1/1, 180/300 SLPM). A 1 h deposition time was sufficient to nearly completely fill the nanopipettes with carbon. The electrostatic discharge (ESD) protection was used during all steps of the electrode preparation to prevent nanometer-scale damage to the tip.[18] The *a* value was validated and the electrode geometry checked by transmission electron microscopy (TEM), using a JEOL JEM-2100 instrument.

SECM Instrumentation and Procedures. SECM experiments were carried out using a home-built instrument, which was similar to that described previously.[19] Briefly, the actuation for imaging and fine positioning was through a P-621 PI Hera 3D nanopositioning stage (Physik Instrumente) driven by an E-725.3CDA multi-axis piezo controller (Physik Instrumente) and controlled by home-written LabView software. A CHI-760 bipotentiostat was used to control the potentials to the tip and substrate and record current during surface approach, scanning and voltammetric experiments. The SECM was mounted on an AVI-200S active vibration isolation platform placed inside a NanoVault acoustic enclosure (Herzan).

To locate a nanoflake, the CNE tip was brought within 1−2 tip radii from the substrate surface as described previously[7,20] and then scanned laterally in the *x*−*y* plane above it. All nanomaterials used in this study are sufficiently conductive to produce an SECM feedback current significantly higher than that measured over the insulating glass support. A coarse electrochemical image based on the higher feedback response was used to locate the center or a nanoflake and position the tip over it. Then, an approach curve was recorded by moving the tip vertically toward the sample. Because the tip radius was always significantly smaller than that of the flake, this protocol ensured that the approach curves were recorded over the nanoobject and not over its edge or the support.

Preparation of Nanoflake Samples. The procedures for synthesis and exfoliation of 2H and 1T/1T′ MoS_2 nanoflakes were adapted from the previous studies.[20,21] The prepared bulk (2H) MoS_2 was solution-exfoliated *via* intercalation with *n*-butyl lithium (2.5 M, Sigma-Aldrich), and the subsequent reaction with water produced nanosheets that were primarily in the 1T MoS_2 phase. To convert 1T/1T′ MoS_2 to 2H phase, it was annealed on glass at 300 °C for 60 min in an inert atmosphere. MoS_2 nanosheets were immobilized on glass slides (Fisher Finest Premium Slides, 25 × 75 × 1 mm) for SECM experiments by a membrane filtration deposition method.[22] Briefly, the exfoliated MoS_2 solution was vacuum-filtrated through a 50 nm pore size polycarbonate membrane, and MoS_2 nanosheets were collected on the membrane. The wet membrane was placed onto a glass slide with MoS_2 side facing the glass. After drying, the polycarbonate membrane was dissolved in chloroform, leaving the MoS_2 nanosheets on the glass surface.

N-doped carbon was synthesized by a dissolution-and-carbonization method, as described previously.[23,24] Briefly, 144 mg of anhydrous glucose and 690 mg of hydroxylammonium chloride were ultrasonically dissolved in 80 mL of deionized water−ethanol solution with a volume ratio of 1:1. Then, the solution was dried at 70 °C overnight, and the obtained powder was calcinated at 600 °C. During the calcination, the glucose was carbonized and then etched by NH_3 produced *via* the decomposition of hydroxylamine hydrochloride precursor to form a N-doped 3-dimensional porous carbon framework.

$Ti_3C_2T_x$ MXene nanosheets with anchored single atomic Ru sites were prepared according to the previously described synthetic procedures.[25] Their structure was confirmed by high-angle annular dark field scanning TEM (HAADF-STEM)

https://doi.org/10.1021/acs.jpcc.1c07309
J. Phys. Chem. C XXXX, XXX, XXX−XXX

imaging and energy dispersive spectroscopy (EDS) mapping. To immobilize N-doped carbon and $Ti_3C_2T_x$ MXene on glass slides, the sample solutions were sonicated for 1 h, and the flakes were deposited onto the glass slide surface by spin coating (Headway Research, Inc.) at 6000 rpm and dried using an IR light source.

RESULTS AND DISCUSSION

Electrochemical Tunneling at Electroactive and Inert Nanoflakes. Tunneling mode current−distance curves obtained with a ∼100 nm CNE tip approaching flat samples are shown in Figure 1. Two kinds of MoS_2 nanoflakes were

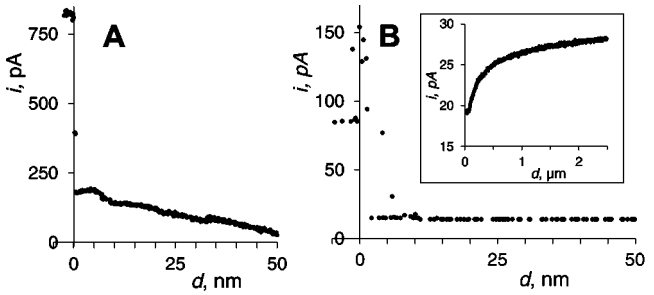

Figure 1. i_T *vs* d curves obtained with a CNE tip approaching (A) 1T and (B) 2H MoS_2 flake attached to the glass surface in 10 mM KCl solution containing 1 mM Fc. Inset: a longer portion of the approach curve showing negative SECM feedback. E_T = 0.4 V *vs* Ag/AgCl; the substrate was unbiased.

used as specimens: a 1T MoS_2 flake (Figure 1A) was metallic/pseudo-metallic, whereas a 2H flake (Figure 1B) was semiconducting and electrochemically inert.[20] Accordingly, positive SECM feedback response at longer separation distances (*i.e.*, d > 2−3 nm) in Figure 1A is due to the regeneration of the ferrocenemethanol (Fc) mediator at the 1T/1T′ flake acting as an unbiased conductive substrate, and negative feedback in Figure 1B (inset) indicates that the 2H flake does not reduce Fc^+ produced at the tip.[20] A sharp increase in i_T occurs in both Figure 1A,B when the tip comes within the tunneling distance (∼3 nm) from the flake surface. The source of the current, however, is totally different. Similar to tunneling experiments at metal NPs,[8,9] the potential of the 1T/1T′ flake changes from the open circuit to the E_T value, and it begins to act as a part of the tip. The high current in Figure 1A is due diffusion of Fc to and its oxidation at the conductive nanoflake whose surface area is much larger than that of the CNE tip; its maximum value is determined by the diffusion current of the redox mediator to the entire flake.

The high tunneling current in Figure 1B flows despite electrochemical inertness of the 2H MoS_2 surface. This current can be attributed to faradaic processes involving the flake material and double layer charging. Because of the transient nature of these processes, the tunneling current drops sharply when the tip continues to slowly push against the flake after making the hard contact with its surface (d < 0 in Figure 1B). By contrast, the current in Figure 1A produced by the steady-state diffusion of Fc levels off after the initial contact (d < 0 in Figure 1A). These data suggest that tunneling mode SECM can be used for probing factors responsible for the apparent electrochemical activity of layered materials other than surface reactivity, for example, lateral and normal (*i.e.*, perpendicular to the flake surface) conductivity. The importance of these factors is well documented, and the high electrical resistance in the normal direction due to low interlayer conductivity has been shown, for example, in MXene flakes.[26]

After bringing a CNE within the tunneling distance from the substrate, single-flake voltammograms were recorded by scanning the tip potential (Figure 2). The steady-state

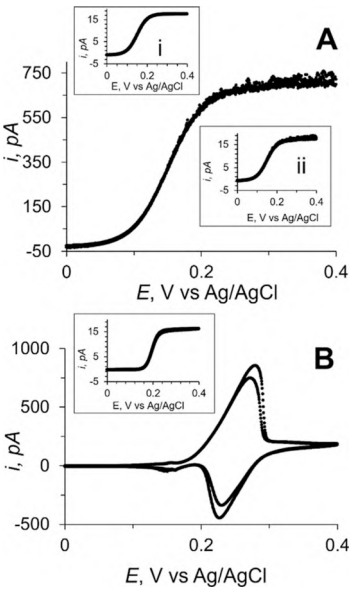

Figure 2. Tunneling mode voltammograms of 1T/1T′ (A) and 2H [(B); two consecutive potential cycles] MoS_2 flakes obtained with CNE tips. The insets show the tip voltammograms in the bulk solution containing 1 mM Fc before [inset i in (A,B)] and after [inset ii in (A)] SECM tunneling experiment. Potential sweep rate, ν = 0.1 V/s.

voltammogram Figure 2A is sigmoidal and retraceable due to the convergent diffusion of Fc to the submicrometer-sized 1T MoS_2 flake. Because the lateral dimensions of the flake are significantly larger that the tip diameter, the diffusion limiting current is much higher than it was either before (inset i) or after (inset ii) the tunneling experiment. Very similar diffusion-limited currents in insets i and ii suggest that the high tunneling current was not caused by CNE damage.

The tunneling mode voltammogram of a 2H MoS_2 flake (Figure 2B) is very different from that in Figure 2A. A pair of non-steady-state voltametric peaks occurs at more positive potentials than the half-wave potential of Fc oxidation. The anodic and cathodic peaks are essentially symmetrical, and their shape is indicative of thin-layer electrochemistry.[27] In contrast to the sigmoidal steady-state voltammogram of Fc oxidation recorded with the same tip far away from the substrate (the inset in Figure 2B), this curve is due to oxidation/reduction of the flake material and double-layer charging. By integrating the current under the anodic and cathodic waves, one can obtain the charge corresponding to these processes. A significant amount of charge passed in Figure 2B suggests sufficiently high lateral and normal conductivity of a 2H MoS_2 flake, whereas its low electrochemical surface reactivity results in slow oxidation of Fc (Figure 2B) and reduction of Fc^+ (Figure 1B).

Probing N-Doped Porous Carbon Catalyst by Tunneling Mode of SECM. N-doped carbon has been widely reported to have high hydrogen evolution reaction (HER) and oxygen evolution reaction (OER) activities.[28−31] Particularly,

https://doi.org/10.1021/acs.jpcc.1c07309
J. Phys. Chem. C XXXX, XXX, XXX−XXX

the doped nitrogen atoms have been reported to be the HER active sties.[28,29] Probing the catalytic activity of micrometer-sized sheets of N-doped porous carbon catalyst by either feedback or generation/collection mode of SECM or SECCM is challenging because of their porosity, significant roughness, and irregular shape (Figure 3).

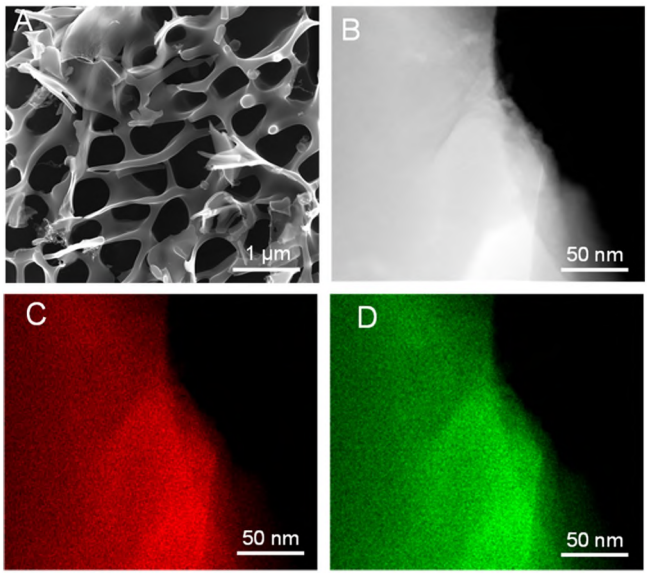

Figure 3. Characterization of N-doped porous carbon. (A) Scanning electron microscopy image. (B) HAADF-STEM image and (C,D) corresponding energy-dispersive X-ray spectroscopy (EDS) mapping of C and N elements.

Electrochemical tunneling experiments provide a relatively straightforward way to probe the activity of a single porous carbon nanosheet. The approach curve in Figure 4A was obtained with a ~70 nm carbon tip and 1 mM ferrocyanide mediator, which unlike ferrocenemethanol is stable in an acidic solution (1 mM $HClO_4$). The sharp transition from the positive feedback response to tunneling occurred over a ~2 nm distance when the tip approached an N-doped porous carbon flake attached the glass surface.

The steady-state voltammogram obtained in the tunneling regime shows oxidation of $Fe(CN)_6^{4-}$ at positive potentials and hydrogen evolution at cathodic potentials (Figure 4B). While a moderate increase in the anodic current (in Figure 4A, the limiting current in the tunneling regime is ~4 times the tip current in solution) corresponds to the ratio of the effective radius of the carbon flake to that of the SECM tip, a very large (orders of magnitude) increase in the cathodic current points to a significant activity of this catalyst toward HER unlike catalytically inert CNE. The slope of the Tafel plot calculated from that voltammogram (286 mV/decade; Figure 4C) is significantly larger than the values typically measured at metal electrodes.

The HER voltammograms measured at an individual N-doped carbon flake can be compared to the ensemble averaged results obtained for a number of flakes immobilized on the surface of a 3 mm glassy carbon electrode (Figure 5A). The background current at the underlying carbon surface and double layer charging as well as the averaging of the responses of different N-doped carbon nanosheets resulted in significant deviations from linearity in the corresponding Tafel plot (Figure 5B). Nevertheless, the cathodic current in Figure 5A is

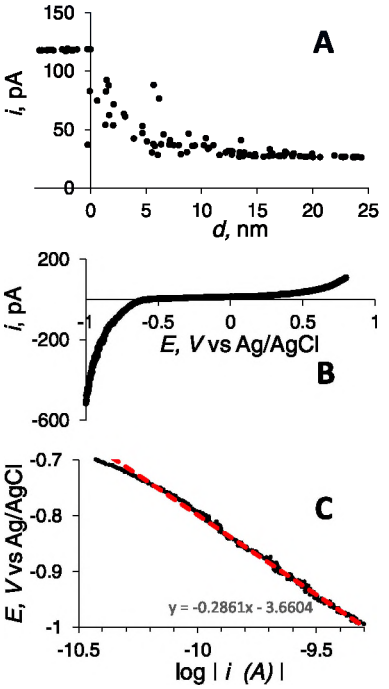

Figure 4. i_T *vs* d curve (A), tunneling mode voltammogram (B), and Tafel plot (C) obtained with a CNE tip approaching an N-doped porous carbon flake attached to the glass surface. Solution contained 10 mM KCl, 1 mM $K_4Fe(CN)_6$, and 1 mM $HClO_4$. (A) E_T = 0.6 V *vs* Ag/AgCl; approach rate was 5 nm/s. (B) ν = 50 mV/s.

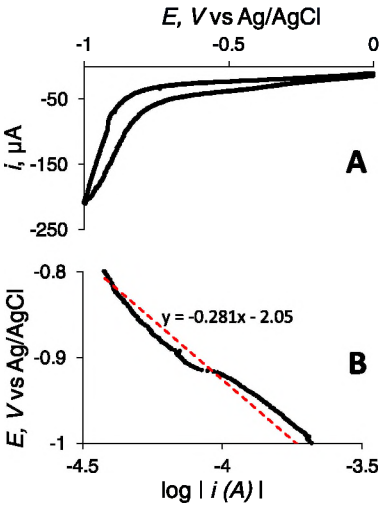

Figure 5. Voltammogram (A) and corresponding Tafel plot (B) of HER at multiple N-doped porous carbon flakes attached to the surface of the 3 mm glassy carbon disk electrode. Solution contained 100 mM KCl and 1 mM $HClO_4$. ν = 50 mV/s.

largely due to the HER at the N-doped carbon surface (the current of $Fe(CN)_6^{4-}$ oxidation occurring at the entire glassy carbon surface is several orders of magnitude higher; not shown), and both the HER onset potential (about −0.6 V) and the Tafel slope (281 mV/decade) in Figure 5 are similar to those in Figure 4.

Comparing Catalytic Activities of Individual MXene Nanoflakes. MXene samples used in our experiments contain single atomic Ru sites anchored onto $Ti_3C_2T_x$ MXene nanosheets (Figure 6) that have been reported to have high

https://doi.org/10.1021/acs.jpcc.1c07309
J. Phys. Chem. C XXXX, XXX, XXX−XXX

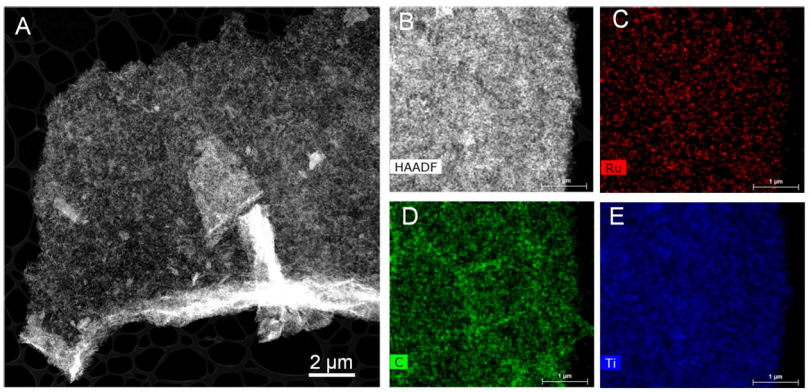

Figure 6. Characterization of single atomic Ru sites anchored onto $Ti_3C_2T_x$ MXene nanosheets. (A) Low-magnification HAADF-STEM image. (B) HAADF-STEM image and (C–E) corresponding EDS mapping of Ru, C, and Ti elements.

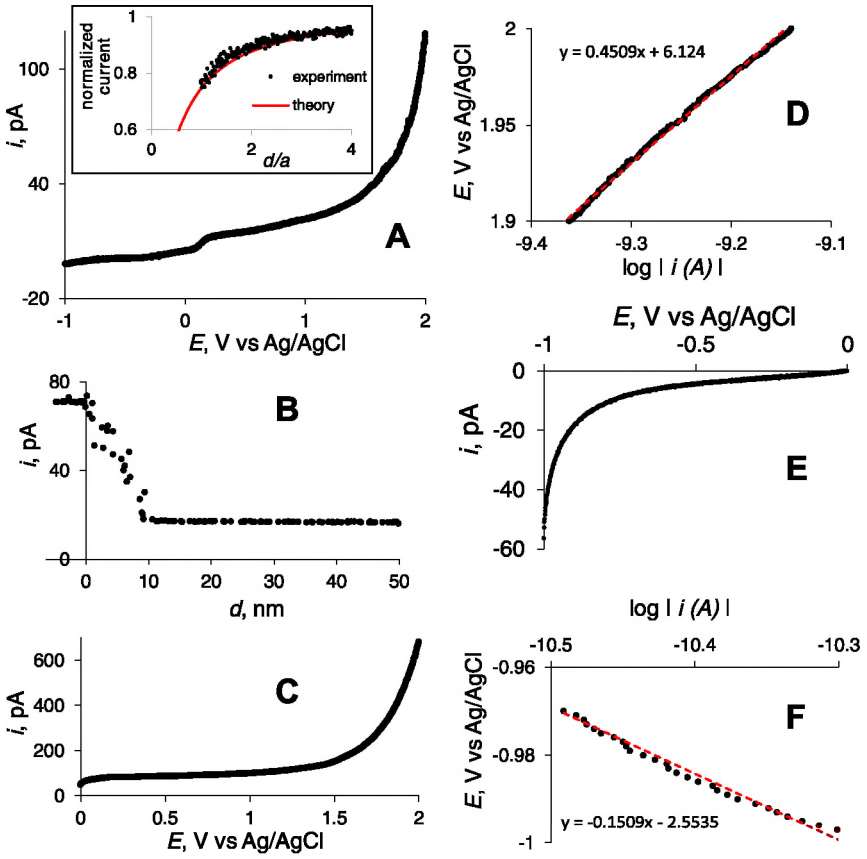

Figure 7. Probing a $Ti_3C_2T_x$ MXene flake with anchored single atomic Ru sites by tunneling mode SECM. (A) Tip voltammogram in the bulk solution and SECM approach curve over glass surface (inset; the experimental current–distance curve is fitted to the negative feedback theory[33]). (B) i_T *vs* d curve obtained with a CNE tip approaching the flake surface. (C,D) Tunneling mode voltammogram of OER at the same flake and corresponding Tafel plot. (E,F) Tunneling mode voltammogram of HER at the same flake and corresponding Tafel plot. Solution contained 1 mM $K_4Fe(CN)_6$, 10 mM KCl, and 1 mM $HClO_4$. (B) E_T = 0.6 V *vs* Ag/AgCl, the substrate was unbiased; 5 nm/s approach velocity.

activity and good stability toward both HER and OER in acidic environments.[25]

A recent study showed that the metal loading and processing conditions can have profound impacts on the electrochemical response of mixed transition metal nitride MXene flakes, modulating the material from semiconducting to metallic.[32] Evaluating the activity of individual MXene flakes from SECM reactivity maps was labor intensive and not quantitative. A single-flake voltammetry can be more efficient for evaluating catalytic activities of individual nanosheets and screening of multiple specimens to optimize their composition and processing conditions. The data shown below address two issues—comparing the catalytic activities of single MXene flakes and reproducibility of the catalytic activity measurements at different locations within the same nanoflake.

We used $Ti_3C_2T_x$ MXene flakes with anchored single atomic Ru sites from two different batches to measure the differences in their catalytic activities for HER and OER. A set of data obtained for a flake from the first batch is shown in Figure 7. The steady-state voltammogram obtained at the carbon tip in the bulk solution containing 1 mM $K_4Fe(CN)_6$ and 1 mM $HClO_4$ over a wide potential range (from −1 to +2 V *vs* Ag/

https://doi.org/10.1021/acs.jpcc.1c07309
J. Phys. Chem. C XXXX, XXX, XXX−XXX

AgCl; Figure 7A) shows the wave of ferrocyanide oxidation and the onset of OER at ~1.5 V. The HER current at $E \geq -1$ V is very low. The tip radius found from the fit of the SECM current−distance curve recorded over the glass surface to the negative feedback theory (the inset in Figure 7A) is a = 44 nm. In Figure 7B, the same tip biased at +0.6 V approaches a $Ti_3C_2T_x$ MXene flake, showing small positive feedback followed by the onset of tunneling. The maximum tunneling current, 71 pA, is only four times the i_T value in the bulk solution, indicating that the MXene flake is relatively small (~400 to 500 nm effective diameter). The voltammogram obtained at the same tip in the tunnelling regime (Figure 7C) shows the limiting current of ferrocyanide close to 71 pA and the OER current ~5 times that in Figure 7A measured at the corresponding potentials. This small increase suggests modest activity of the investigated flake for OER in agreement with a large Tafel slop (450 mV/decade) in Figure 7D. By contrast, the HER current at the flake (Figure 7E) is orders of magnitude higher than that at the carbon tip (Figure 7A), and the Tafel slope (150 mV/decade; Figure 7F) is significantly smaller.

The reproducibility of tunneling mode measurements can be evaluated by comparing the above results to those shown in Figure 8 in which the same carbon SECM tip approached the same $Ti_3C_2T_x$ MXene flake surface at a different spot, about 100 nm from that probed in Figure 7. The maximum tunneling current is Figure 8A (71 pA) is the same as the value in Figure 7B.

This value represents the steady-state diffusion-limited current of ferrocyanide ions to the entire flake surface (the blocking effect of the tip body is similar in both cases). The OER and HER voltammograms (Figure 8B,C) and Tafel plots (insets in Figure 8B,C) are also very similar to the corresponding data in Figure 7. The high reproducibility of the data measured at different locations is apparently related to the uniform catalytic activity of the MXene flake surface inferred previously from SECM reactivity maps.[32]

The data obtained with a $Ti_3C_2T_x$ MXene sample from the second batch are shown in Figure 9. From the voltammogram in Figure 9A and the fit of the experimental approach curve to the theory (the inset), the tip radius is 61 nm. The MXene flake is significantly larger than that probed in Figures 7 and 8. From the maximum tunneling current in Figure 9B, the effective flake diameter is ~1.2 μm, that is, 2−3 times that in Figures 7 and 8. Thus, the current density of OER (Figure 9B) is comparable to that in Figures 7C and 8, and the overall OER activity of this flake is comparable to (or slightly lower than) that of a flake from the first batch.

Unlike OER, the current density of HER in Figure 9D is at least one order of magnitude higher than that measured at the corresponding potentials in Figures 7E and 8C. The overall activity of this flake to HER is much higher, suggesting that different active sites on the surface of the same $Ti_3C_2T_x$ MXene flake are responsible for OER and HER catalysis.

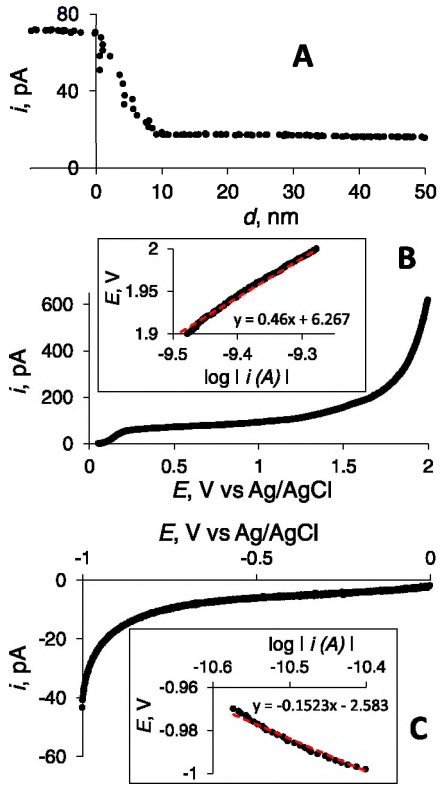

Figure 8. Tunneling mode SECM measurements at a different location of the $Ti_3C_2T_x$ MXene flake probed in Figure 7 using the same CNE tip. (A) i_T *vs* d curve obtained with a CNE tip approaching the flake surface. (B) Tunneling mode voltammogram of OER and corresponding Tafel plot (the inset). (C) Tunneling mode voltammogram of HER and corresponding Tafel plot (the inset). For experimental parameters, see Figure 7.

CONCLUSIONS

We demonstrated the possibility of electrochemical tunneling experiments at flat nanoflakes and used this technique to probe nanosheet specimens with different size, geometry, conductivity, and surface reactivity. A small physical size of a CNE (including a very thin insulating sheath) allows for its conductive core to be brought within the tunneling distance (<3 nm) from the flat surface, which would be hard to do with a glass-sealed metal tip surrounded by a thicker insulating sheath. Another important advantage of the needle-like CNE geometry is a relatively minor blocking of redox species diffusion to the nanoflake surface by the tip body.

Tunneling mode voltammetry allows one to characterize activity, conductivity, and charging properties of a single flake and faradaic processes in layered nanomaterials without making direct ohmic contact with them. This single entity electrochemical technique, which measures the properties of single nanomaterials without ensemble averaging, provides relatively straightforward means for comparing electrocatalytic activities of individual nanoflakes. Our finding that two $Ti_3C_2T_x$ MXene flakes with anchored single atomic Ru sites have comparable activities toward OER and completely different activities for HER provides a strong evidence that these processes occur on different active sites.

Single-flake voltammetry is conceptually somewhat like SECCM[5] because both techniques measure the current flowing at a nanoscale sample area. An advantage of tunneling SECM experiments is in a very small (atomic scale) contact area that enables probing both small and relatively large and rough samples that do not have to be attached to a conductive support. The signal is produced by the entire nanoflake without the uncertainty of the liquid meniscus contact area and the need to discriminate between the contributions of the

https://doi.org/10.1021/acs.jpcc.1c07309
J. Phys. Chem. C XXXX, XXX, XXX−XXX

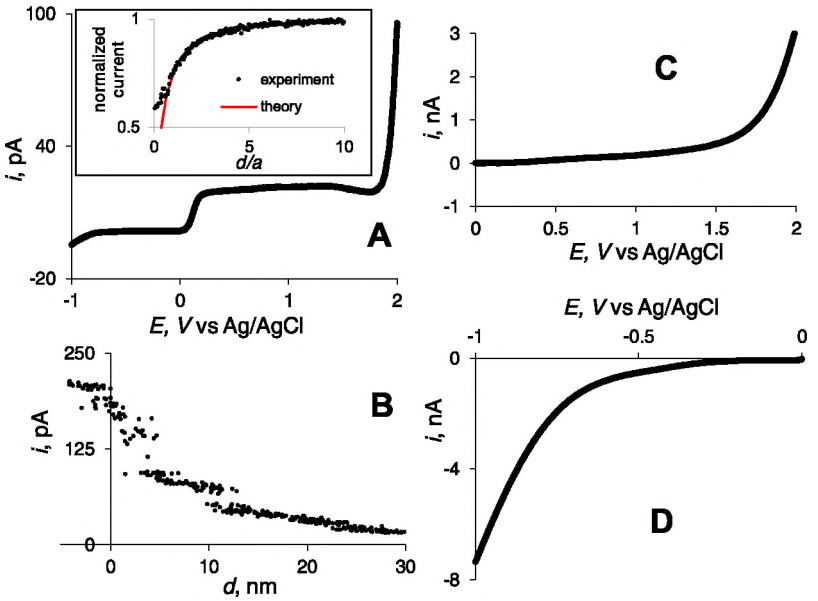

Figure 9. Tunneling mode SECM measurements at a different $Ti_3C_2T_x$ MXene flake with anchored single atomic Ru sites. (A) Tip voltammogram in the bulk solution and SECM approach curve over glass surface (inset; the experimental current−distance curve is fitted to the negative feedback theory[33]). (B) i_T *vs d* curve obtained with a CNE tip approaching the flake surface. Tunneling mode voltammograms of OER (C) and HER (D) recorded at the same tip electrode touching the same flake. For experimental parameters, see Figure 7.

specimen and the underlying conductive surface to the measured current.

Tunneling mode voltammetry addresses the entire nanoflake as a single entity without probing possible heterogeneity of its surface reactivity. When the nanoflake properties are essentially uniform, electrochemical tunneling experiments at different spots of the same flake produce very similar results (*cf.* Figures 7 and 8). If the flake reactivity and/or conductivity are substantially non-uniform, the tunneling barrier and measured tunneling current may vary over its surface. The possibility of using tunneling mode of SECM for high-resolution reactivity mapping is currently explored in our laboratories.

AUTHOR INFORMATION

Corresponding Author

Michael V. Mirkin − *Department of Chemistry and Biochemistry, Queens College, Flushing, New York 11367, United States; The Graduate Center of CUNY, New York, New York 10016, United States;* orcid.org/0000-0002-3424-5810; Email: mmirkin@qc.cuny.edu; Fax: 718-997-5531

Authors

Tianyu Bo − *Department of Chemistry and Biochemistry, Queens College, Flushing, New York 11367, United States; The Graduate Center of CUNY, New York, New York 10016, United States*

Xiang Wang − *Department of Chemistry and Biochemistry, Queens College, Flushing, New York 11367, United States; The Graduate Center of CUNY, New York, New York 10016, United States;* orcid.org/0000-0002-9558-7849

Rui Jia − *Department of Chemistry and Biochemistry, Queens College, Flushing, New York 11367, United States; The Graduate Center of CUNY, New York, New York 10016, United States;* orcid.org/0000-0002-6094-982X

Lili Han − *Department of Physics & Astronomy, University of California, Irvine, Irvine, California 92697, United States*

Huolin L. Xin − *Department of Physics & Astronomy, University of California, Irvine, Irvine, California 92697, United States;* orcid.org/0000-0002-6521-868X

Hanyu Zhang − *Materials, Chemistry, and Computational Science Directorate, National Renewable Energy Laboratory, Golden, Colorado 80401, United States*

Elisa M. Miller − *Materials, Chemistry, and Computational Science Directorate, National Renewable Energy Laboratory, Golden, Colorado 80401, United States;* orcid.org/0000-0002-7648-5433

Complete contact information is available at: https://pubs.acs.org/10.1021/acs.jpcc.1c07309

Author Contributions

The manuscript was written through contributions of all authors. All authors have given approval to the final version of the manuscript.

Notes

The authors declare no competing financial interest.

ACKNOWLEDGMENTS

The support of this work by the National Science Foundation (CHE-2102298 to M.V.M. and CHE-1900401 to H.L.X.) is gratefully acknowledged. H.Z. and E.M.M. acknowledge funding provided by U.S Department of Energy, Office of Science, Office of Basic Energy Sciences, Division of Chemical Sciences, Geosciences and Biosciences, Solar Photochemistry. The NREL authors would like to thank the Alliance for Sustainable Energy, LLC, the manager and operator of the National Renewable Energy Laboratory for the U.S. Department of Energy under contract no. DE-AC36-08GO28308. The views expressed in the article do not necessarily represent the views of the Department of Energy or the U.S. Government. The U.S. Government retains and the publisher, by accepting the article for publication, acknowledges that the U.S. Government retains a nonexclusive, paid-up, irrevocable, worldwide license to publish or reproduce the published form

https://doi.org/10.1021/acs.jpcc.1c07309
J. Phys. Chem. C XXXX, XXX, XXX−XXX

of this work, or allow others to do so, for U.S. Government purposes.

REFERENCES

(1) Amemiya, S. Nanoscale Scanning Electrochemical Microscopy *Electroanalytical Chemistry*; Bard, A. J., Zoski, C. G., Eds.; CRC Press, 2015; Vol. *26*, pp 1−72.

(2) Kai, T.; Zoski, C. G.; Bard, A. J. Scanning electrochemical microscopy at the nanometer level. *Chem. Commun.* **2018**, *54*, 1934−1947.

(3) Wang, X.; Askarova, G.; Mirkin, M. V. Electrochemical Microscopy at the Nanoscale. In *Nanoscale Electrochemistry*; Wain, A., Dickinson, E., Eds.; Elsevier Ltd., 2021; pp 129−202.

(4) Bard, A. J.; Fan, F. R. F.; Kwak, J.; Lev, O. Scanning electrochemical microscopy. Introduction and principles. *Anal. Chem.* **1989**, *61*, 132−138.

(5) Ebejer, N.; Guell, A. G.; Lai, S. C. S.; McKelvey, K.; Snowden, M. E.; Unwin, P. R. Scanning Electrochemical Cell Microscopy: A Versatile Technique for Nanoscale Electrochemistry and Functional Imaging. *Annu. Rev. Anal. Chem.* **2013**, *6*, 329−351.

(6) Mariano, R. G.; McKelvey, K.; White, H. S.; Kanan, M. W. Selective Increase in CO_2 Electroreduction Activity at Grain-boundary Surface Terminations. *Science* **2017**, *358*, 1187−1192.

(7) Sun, T.; Wang, D.; Mirkin, M. V.; Cheng, H.; Zheng, J.-C.; Richards, R. M.; Lin, F.; Xin, H. L. Direct High-Resolution Mapping of Electrocatalytic Activity of Semi-Two-Dimensional Catalysts with Single-Edge Sensitivity. *Proc. Natl. Acad. Sci. U.S.A.* **2019**, *116*, 11618−11623.

(8) Sun, T.; Wang, D.; Mirkin, M. V. Tunneling mode of scanning electrochemical microscopy: probing electrochemical processes at single nanoparticles. *Angew. Chem., Int. Ed.* **2018**, *57*, 7463−7467.

(9) Sun, T.; Wang, D.; Mirkin, M. V. Electrochemistry at a Single Nanoparticle: from Bipolar Regime to Tunnelling. *Faraday Discuss.* **2018**, *210*, 173−188.

(10) Blanchard, P.-Y.; Sun, T.; Yu, Y.; Wei, Z.; Matsui, H.; Mirkin, M. V. Scanning Electrochemical Microscopy Study of Permeability of a Thiolated Aryl Multilayer and Imaging of Single Nanocubes Anchored to It. *Langmuir* **2016**, *32*, 2500−2508.

(11) Xu, B.; Tao, N. J. Measurement of Single-Molecule Resistance by Repeated Formation of Molecular Junctions. *Science* **2003**, *301*, 1221−1223.

(12) Pfisterer, J. H. K.; Liang, Y.; Schneider, O.; Bandarenka, A. S. Direct instrumental identification of catalytically active surface sites. *Nature* **2017**, *549*, 74−77.

(13) Edmondson, J. F.; Meloni, G. N.; Costantini, G.; Unwin, P. R. Synchronous Electrical Conductance- and Electron Tunnelling-Scanning Electrochemical Microscopy Measurements. *ChemElectroChem* **2020**, *7*, 697−706.

(14) Wang, X.; Wang, Y.-Q.; Feng, Y.-C.; Wang, D.; Wan, L.-J. Insights into electrocatalysis by scanning tunnelling microscopy. *Chem. Soc. Rev.* **2021**, *50*, 5832−5849.

(15) Barman, K.; Wang, X.; Jia, R.; Mirkin, M. V. Mediated Charge Transfer at Nanoelectrodes: A New Approach to Electrochemical Reactivity Mapping and Nanosensing. *J. Am. Chem. Soc.* **2021**, *143*, 8547−8551.

(16) Singhal, R.; Bhattacharyya, S.; Orynbayeva, Z.; Vitol, E.; Friedman, G.; Gogotsi, Y. Small diameter carbon nanopipettes. *Nanotechnology* **2010**, *21*, 015304.

(17) Yu, Y.; Gao, Y.; Hu, K.; Blanchard, P.-Y.; Noël, J.-M.; Nareshkumar, T.; Phani, K. L.; Friedman, G.; Gogotsi, Y.; Mirkin, M. V. Electrochemistry and Electrocatalysis at Single Gold Nanoparticles Attached to Carbon Nanoelectrodes. *ChemElectroChem* **2015**, *2*, 58−63.

(18) Nioradze, N.; Chen, R.; Kim, J.; Shen, M.; Santhosh, P.; Amemiya, S. Origins of nanoscale damage to glass-sealed platinum electrodes with submicrometer and nanometer size. *Anal. Chem.* **2013**, *85*, 6198−6202.

(19) Bae, J. H.; Brocenschi, R. F.; Kisslinger, K.; Xin, H. L.; Mirkin, M. V. Dissolution of Pt during Oxygen Reduction Reaction Produces Pt Nanoparticles. *Anal. Chem.* **2017**, *89*, 12618−12621.

(20) Sun, T.; Zhang, H.; Wang, X.; Liu, J.; Xiao, C.; Nanayakkara, S. U.; Blackburn, J. L.; Mirkin, M. V.; Miller, E. M. Nanoscale mapping of hydrogen evolution on metallic and semiconducting MoS_2 nanosheets. *Nanoscale Horiz.* **2019**, *4*, 619−624.

(21) Benson, E. E.; Zhang, H.; Schuman, S. A.; Nanayakkara, S. U.; Bronstein, N. D.; Ferrere, S.; Blackburn, J. L.; Miller, E. M. Balancing the Hydrogen Evolution Reaction, Surface Energetics, and Stability of Metallic MoS_2 Nanosheets via Covalent Functionalization. *J. Am. Chem. Soc.* **2018**, *140*, 441−450.

(22) Zhang, H.; Choi, J.; Ramani, A.; Voiry, D.; Natoli, S. N.; Chhowalla, M.; McMillin, D. R.; Choi, J. H. Engineering Chemically Exfoliated Large-Area Two-Dimensional MoS_2 Nanolayers with Porphyrins for Improved Light Harvesting. *ChemPhysChem* **2016**, *17*, 2854−2862.

(23) Han, L.; Liu, X.; Chen, J.; Lin, R.; Liu, H.; Lu, F.; Bak, S.; Liang, Z.; Zhao, S.; Stavitski, E.; et al. Atomically Dispersed Molybdenum Catalysts for Efficient Ambient Nitrogen Fixation. *Angew. Chem., Int. Ed.* **2019**, *58*, 2321−2325.

(24) Han, L.; Song, S.; Liu, M.; Yao, S.; Liang, Z.; Cheng, H.; Ren, Z.; Liu, W.; Lin, R.; Qi, G.; et al. Stable and Efficient Single-Atom Zn Catalyst for CO_2 Reduction to CH_4. *J. Am. Chem. Soc.* **2020**, *142*, 12563−12567.

(25) Peng, X.; Zhao, S.; Mi, Y.; Han, L.; Liu, X.; Qi, D.; Sun, J.; Liu, Y.; Bao, H.; Zhuo, L.; et al. Trifunctional Single-Atomic Ru Sites Enable Efficient Overall Water Splitting and Oxygen Reduction in Acidic Media. *Small* **2020**, *16*, 2002888.

(26) Hantanasirisakul, K.; Gogotsi, Y. Electronic and Optical Properties of 2D Transition Metal Carbides and Nitrides (MXenes). *Adv. Mater.* **2018**, *30*, 1804779.

(27) Bard, A. J.; Faulkner, L. R. *Electrochemical Methods: Fundamentals and Applications*, 2nd ed.; John Wiley & Sons: New York, 2001; Section 11.7.

(28) Long, G.-f.; Wan, K.; Liu, M.-y.; Liang, Z.-x.; Piao, J.-h.; Tsiakaras, P. Active sites and mechanism on nitrogen-doped carbon catalyst for hydrogen evolution reaction. *J. Catal.* **2017**, *348*, 151−159.

(29) Qu, K.; Zheng, Y.; Zhang, X.; Davey, K.; Dai, S.; Qiao, S. Z. Promotion of Electrocatalytic Hydrogen Evolution Reaction on Nitrogen-Doped Carbon Nanosheets with Secondary Heteroatoms. *ACS Nano* **2017**, *11*, 7293−7300.

(30) Wang, H.; Yi, Q.; Gao, L.; Gao, Y.; Liu, T.; Jiang, Y.-B.; Sun, Y.; Zou, G. Hierarchically interconnected nitrogen-doped carbon nanosheets for an efficient hydrogen evolution reaction. *Nanoscale* **2017**, *9*, 16342−16348.

(31) Zhao, Y.; Nakamura, R.; Kamiya, K.; Nakanishi, S.; Hashimoto, K. Nitrogen-doped carbon nanomaterials as non-metal electrocatalysts for water oxidation. *Nat. Commun.* **2013**, *4*, 2390.

(32) Djire, A.; Wang, X.; Xiao, C.; Nwamba, O. C.; Mirkin, M. V.; Neale, N. R. Basal Plane Hydrogen Evolution Activity from Mixed Metal Nitride MXenes Measured by Scanning Electrochemical Microscopy. *Adv. Funct. Mater.* **2020**, *30*, 2001136.

(33) Cornut, R.; Lefrou, C. A unified new analytical approximation for negative feedback currents with a microdisk SECM tip. *J. Electroanal. Chem.* **2007**, *608*, 59−66.

https://doi.org/10.1021/acs.jpcc.1c07309
J. Phys. Chem. C XXXX, XXX, XXX−XXX